



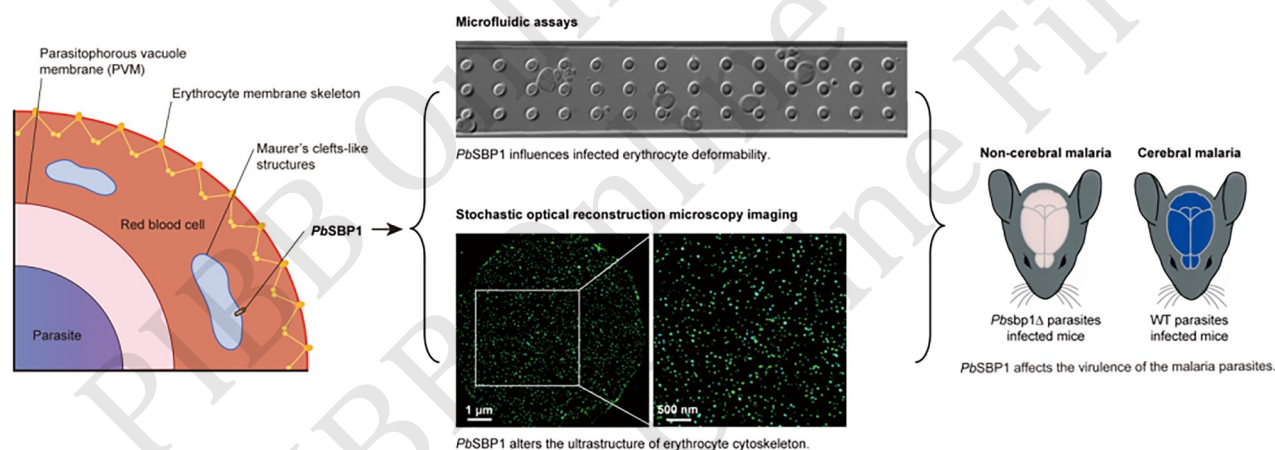
Skeleton Binding Protein 1 of *Plasmodium berghei* Influences Deformability and Cytoskeletal Ultrastructure of Infected Erythrocyte*

GUO Xin-Yue¹⁾, ZHAO Huan-Qi¹⁾, ZHONG Yan-Xuan¹⁾, JIANG Ru-Meng¹⁾, LI Yao-Xian²⁾, PAN Lei-Ting²⁾, WANG Qian^{1)**}, SHI Xiao-Yu^{1)**}

¹⁾Department of Immunology, School of Basic Medical Sciences, Tianjin Medical University, Tianjin Key Laboratory of Cellular and Molecular Immunology, Key Laboratory of Immune Microenvironment and Diseases of Educational Ministry of China, Tianjin 300070, China;

²⁾The Key Laboratory of Weak-Light Nonlinear Photonics of Education Ministry, School of Physics and TEDA Institute of Applied Physics, Nankai University, Tianjin 300071, China)

Graphical abstract



Abstract Objective The malaria parasites remodel the host erythrocyte structure by exporting parasite proteins that interact with the membrane skeleton proteins of red blood cells (RBCs), facilitating their intracellular survival and pathogenicity. Skeleton-binding protein 1 (SBP1) is a conserved exported protein across *Plasmodium* species. In *Plasmodium falciparum*, SBP1 has been reported to interact with erythrocyte membrane skeleton proteins 4.1R and spectrin, while its contribution to erythrocyte remodeling and parasite virulence in *Plasmodium berghei* (*Pb*) remains unclear. This study aims to determine whether *PbSBP1* associates with the host cytoskeletal protein 4.1R and to investigate its role in the remodeling of host RBCs and the pathogenicity of *Plasmodium berghei*. **Methods** In *Plasmodium berghei*, the relationship between *PbSBP1* and the erythrocyte cytoskeletal protein 4.1R was examined using co-immunoprecipitation. A *Pbsbp1* gene knockout mutant of *Plasmodium berghei* (*Pbsbp1*Δ) was generated based on the principle of double crossover homologous recombination. The deformability of erythrocytes infected with *Pbsbp1*Δ parasites

* This work was supported by grants from The National Natural Science Foundation of China (32200976, 32070701).

** Corresponding author.

WANG Qian. Tel: 86-22-83336817, E-mail: wangq@tmu.edu.cn

SHI Xiao-Yu. Tel: 86-22-83336817, E-mail: shixy@tmu.edu.cn

Received: January 6, 2026 Accepted: March 1, 2026

was assessed using microfluidic methods. Microchannels with an array of cylindrical pillars were used to detect modifications in infected RBC deformability. The infected RBCs were squashed between the rows and recovered between the columns and the transit velocity ($\mu\text{m/s}$) of infected RBCs travelling through the microchannel was recorded. The component of the erythrocyte membrane skeleton junctional complex, tropomodulin (TMOD), was fluorescently labeled, and the cytoskeletal network of infected erythrocytes was imaged using super-resolution stochastic optical reconstruction microscopy (STORM) to analyze ultrastructural changes in the cytoskeleton of wild-type (WT) and *Pbsbp1* Δ -infected erythrocytes. Actin-based junctional complexes were displayed as individual clusters by the labeled TMOD in the STORM images, and the cluster densities and distances between adjacent clusters of infected RBCs were calculated. Additionally, rodent malaria models (BALB/c mice) and experimental cerebral malaria models (C57BL/6 mice) were employed to monitor the growth of *Pbsbp1* Δ and WT parasites during the intraerythrocytic stage and their capacity to induce cerebral malaria in mice. **Results** *PbSBP1* may participate in the remodeling of infected erythrocytes through direct or indirect interaction with the erythrocyte cytoskeletal protein 4.1R. Microfluidic assays revealed that the deformability of erythrocytes infected with *Pbsbp1* Δ parasites was significantly enhanced compared to those infected with WT parasites. STORM imaging further demonstrated that the ultrastructure of the erythrocyte cytoskeleton in *Pbsbp1* Δ -infected cells was altered relative to that in WT-infected erythrocytes. The distances between nearest neighbors of clusters had a tendency to increase while the cluster densities were decreased in *Pbsbp1* Δ -infected RBCs compared to WT-infected RBCs. Subsequent phenotypic analysis indicated that the growth rate of *Pbsbp1* Δ parasites during the intraerythrocytic stage was significantly slower than that of WT parasites, and their ability to induce cerebral malaria in mice was also attenuated. These findings suggest that *PbSBP1* is involved in the remodeling of the erythrocyte membrane skeleton, likely through its direct or indirect interaction with protein 4.1R, thereby regulating the deformability of infected erythrocytes and influencing the pathogenicity of the blood-stage parasites. **Conclusion** This study establishes a role for *PbSBP1* in host erythrocyte remodeling and parasite virulence, providing new research strategies for the prevention and treatment of malaria.

Key words *PbSBP1*, erythrocyte remodeling, cytoskeletal ultrastructure, erythrocyte deformability

DOI: 10.3724/j.pibb.2026.0010

CSTR: 32369.14.pibb.20260010

Under normal physiological conditions, erythrocytes exhibit a high degree of deformability, which is attributed to the large surface area relative to volume, moderate viscosity of cytoplasm, and the elasticity of the membrane cytoskeleton. The structural organization of the erythrocyte membrane skeleton is composed of a two-dimensional triangular network, which is formed by spectrin tetramers connected by junctional complexes consisting of F-actin, protein 4.1, adducin, tropomodulin, and other associated proteins^[1]. This cytoskeleton network is anchored to the erythrocyte plasma membrane by two molecular complexes of membrane proteins, ankyrin-based complex and protein 4.1R-based complex. Membrane proteins band 3 and Rh-associated glycoprotein (RhAG) connect the lipid bilayer with the membrane skeleton via interaction with ankyrin, while glycophorin C, XK, Rh, and Duffy achieve this connection through their interactions with protein 4.1R. The erythrocyte membrane skeleton network and its connection with the plasma membrane is the structural basis for maintaining the elasticity of the erythrocyte, which is also the major target for

modification during *Plasmodium* infection.

After infection with malaria parasites, the red blood cell (RBC) is remodeled strikingly by parasite-exported proteins, which is crucial for the pathogenesis of malaria infection and the transfer of virulence factors to the RBC surface. Some of the parasite exported proteins are released to bind with RBC membrane skeleton, leading to loss of biconcave shape and increased rigidity of erythrocytes^[2]. In *Plasmodium falciparum* (*Pf*), some exported proteins have been reported to target the erythrocyte cytoskeleton, including ring-infected erythrocyte surface antigen (RESA)^[3], mature parasite-infected erythrocyte surface antigen (MESA)^[4-5], knob-associated histidine-rich protein (KAHRP)^[6-7], *P. falciparum* erythrocyte membrane protein 1 (*PfEMP1*)^[8], *PfEMP3*^[9], PFE1605w (LyMP/PFD37_0532400)^[10], *P. falciparum* protein 332 (*Pf332*)^[11], PF3D7_0402000^[12], PF3D7_1401600^[13], and *P. falciparum* skeleton-binding protein 1 (*PfSBP1*)^[14]. The interaction between parasite exported proteins and erythrocyte membrane skeleton may influence interactions between cytoskeletal proteins, disrupt the

actin-based junctional complex and cross-link spectrin, resulting in dramatic changes of membrane surface topography (knob formation) and skeleton structure.

Protein 4.1R plays a crucial role in promoting the binding between spectrin and actin, and it also participates in anchoring the membrane skeleton to the lipid bilayer. MESA, PF3D7_0402000, PF3D7_1401600, and *PfSBP1* have been proven to have interactions with protein 4.1R^[4, 12-14]. *PfSBP1* is located in Maurer's cleft and interacts with erythrocyte membrane skeleton by binding to protein 4.1R and spectrin^[14]. SBP1 is a conserved protein among *Plasmodium* species and *Plasmodium berghei* (*Pb*) SBP1 executes similar function as *PfSBP1*^[15]. *PbSBP1* also localizes in Maurer's clefts-like structures in *P. berghei*-infected RBCs and co-localizes with IBIS1^[15-16]. In this study, we began with the interaction of *PbSBP1* and protein 4.1R, and constructed the *Pbsbp1* knockout parasite line (*Pbsbp1* Δ). Then we mainly focused on the role of *PbSBP1* in remodeling of infected erythrocyte, found that the deformability was increased and the skeleton architecture was modified in *Pbsbp1* Δ-infected RBCs compared with wild type (WT)-infected RBCs. We also investigated the function of *PbSBP1* in the pathogenesis of blood stage parasites, and found that the growth of *Pbsbp1* Δ parasite slowed down, and its ability to induce cerebral malaria also decreased. These results indicate that *PbSBP1* may contribute to the remodeling of erythrocyte membrane skeleton architecture by interaction with protein 4.1R directly or indirectly, which is associated with its function in the pathogenicity of the malaria parasite.

1 Materials and methods

1.1 Animals and Malaria parasites

Female Wistar rats weighing 50–70 g, female BALB/c mice aged 4–6 weeks and female C57BL/6 mice aged 6–8 weeks were purchased from SPF (Beijing) Biotechnology Co. Ltd. All animal experiments and husbandry were conducted under the guidelines of Tianjin Medical University (TMU) IACUC. *Plasmodium berghei* ANKA line was used in all experiments. Rats or mice were infected with *P. berghei* and Giemsa staining of a thin blood smear was used to measure parasitemia and determine the malaria stage.

1.2 Isolation of membranes of *P. berghei*-infected erythrocytes

Membranes of infected red blood cells (iRBCs) were prepared according to a previously reported method with slight modifications^[17]. The blood was collected from *P. berghei* ANKA WT-infected rat with a > 20% parasitemia via cardiac puncture under terminal anesthesia. White cells were removed from the blood through two-layered columns composed of acid-washed glass beads and CF 11 cellulose, then the schizont stage cells were purified by histodenz density gradient centrifugation. Thereafter, the isolated samples were resuspended in ACK lysis buffer to lyse RBCs and centrifuged (400g, 10 min, 4°C). The supernatant was collected and transferred to a new 50 ml centrifuge tube, and the pellets were repeatedly lysed with ACK lysis buffer until the supernatant appeared colorless. All the obtained supernatant was centrifuged in 50 ml tube (10 000g, 20 min, 4°C) and the pellets containing ghost membranes and a small amount of parasites were transferred to a 1.5 ml Eppendorf tube. Centrifugation was then increased to 20 000g (20–30 min, 4°C) and the upper layer of sediment containing the yellow-whitish ghost membranes was isolated and washed several times until the ghost membranes appeared yellow-whitish. The membranes of iRBCs were stored at –80°C.

1.3 Generation of anti-*PbSBP1* antibody

This anti-*PbSBP1* antibody was prepared by GL Biochem (Shanghai) Ltd. (Shanghai, China). Three *PbSBP1* peptides (YAPESIASNILLDSFSTKPQ-Cys, Cys-KPPNPLKLFLSQYDISPHGR, Cys-DSPYNAQPPTSIQSDN) localized at the N-terminus or C-terminus of the protein sequence, were used as immunogens to raise antisera. All three peptides were mixed and injected into the same rabbit, and the antisera were purified by affinity chromatography to generate polyclonal antibodies. The antibody was tested at a 1:500 dilution as the primary antibody for Western blotting.

1.4 Recombinant protein *PbSBP1* expression in *Escherichia coli*

The cDNA sequence of *Pbsbp1* tagged with a flag was first codon-optimized for *Escherichia coli* (*E. coli*) and synthesized by GENEWIZ (Suzhou, China). Then the synthesized cDNA fragment was cloned into vector pET-28a (+). The expression plasmid was transformed into BL21 (DE3) chemically

competent cells. The cells were plated on the antibiotic selection plate and incubated overnight at 37°C. The single clone was selected and resuspended in 3 ml liquid culture with kanamycin, and incubated at 37°C with shaking until the OD₆₀₀ reached 0.4–0.8. Then the culture was added with IPTG (500 μmol/L final concentration) or not and incubated with shaking overnight at 16°C. Proteins were extracted from the cell pellets of 500 μl bacterial culture. The cell pellets were resuspended in 100 μl H₂O and added with 25 μl 5×loading buffer (containing β-mercaptoethanol). The lysates were heated at 95°C for 10 min and cooled on ice before Western blotting.

1.5 Co-immunoprecipitation

For immunoprecipitation of erythrocyte cytoskeleton protein 4.1R, membrane protein extracts of iRBCs were prepared by solubilization in RIPA buffer (Sigma, R0278) supplemented with protease inhibitor cocktail (Roche, 04693116001) for 30 min on ice with repeated pipetting. The supernatant of lysate was separated by centrifugation at 13 000g for 10 min at 4°C. The mouse anti-4.1R antibody (Santa Cruz Biotechnology, sc-166759) or the normal mouse IgG (Bioss, bs-0296P) were incubated with Protein A/G magnetic beads (Sino Biological, BAG001) at 4°C for 2 h, then incubated with the membrane extracts for 4 h at 4°C. The magnetic beads with precipitated immunocomplexes were resuspended in elution buffer and 5×SDS-PAGE loading buffer and incubated at 65°C for 15 min, and the supernatant was assayed by Western blot analysis with anti-*PbsBP1* antibody (1:500 dilution).

1.6 Plasmid construction and malaria transfection

To delete *Pbsbp1* (PBANKA_1101300) in *P. berghei* genome, plasmid pL0035-*Pbsbp1* Δ was constructed. pL0035-*Pbsbp1* Δ contains a DHFR-yfcu cassette flanked by 1 129 bp and 1 000 bp sequences from 5' and 3' end of the SBP1 coding sequence. *EcoRI* and *HindIII* linearized pL0035-*Pbsbp1* Δ was used to transfect *P. berghei* ANKA schizonts according to the standard methodology^[18]. The transfectant was selected using pyrimethamine and single clones of *Pbsbp1* Δ parasites were screened by limiting dilution.

1.7 Genotype identification of *Pbsbp1*Δ parasite

Genomic DNA (gDNA) was extracted from the parasites by QIAamp DNA Mini Kit (QIAGEN,

51306). The genotype of the selected parasite was determined by PCR and Southern blotting. PCR primers used to confirm integration are listed as follows: P305 and P306 are used to identify wild type (P305: 5'-GAAGCAGCACAAGCGGAACAAGT, P306: 5'-GGCCTTTTTGTTATGTTTACTTGC), GW1 and P307 are used to identify *Pbsbp1*Δ (GW1: 5'-CATACTAGCCATTTTATGTG, P307: 5'-AGCACGTTGTGAAAATACTC). Southern blotting was performed as previously described^[19]. Genomic DNAs of WT and *Pbsbp1* Δ were digested with *SpeI* and *EcoRI*, and primers used for probe amplification are 5'-GGATATAAAATTATAAAAAGTTATTTAATGTAAAG (F) and 5'-CCGAATTAATCTTCTTAAGAGAAAGTTTTTTTGATGC (R).

1.8 Infected erythrocytes deformability measurement by microfluidic approach

A microfluidic assembly was previously designed to test erythrocyte deformability^[20], so we utilized this method to measure the deformability of iRBCs. The microchannel with array of cylindrical pillars was used to quantify the modifications of iRBC deformability. The diameter of normal RBC is ~7 μm, which can pass smoothly through the microchannel rows that are 3 μm apart. Due to the enlarged size of schizont infected RBC compared with normal RBC, the iRBCs are blocked by the 3 μm-wide microchannel as they pass through. Thus, distances between the rows and the columns in the micropillar array we chose to evaluate iRBCs deformability were 6 μm and 10 μm. The diameter of the pillar is 6 μm. Schizont-infected erythrocytes were isolated by histodenz density gradient centrifugation. The purified iRBCs squeezed themselves between the pillars and then recovered between the columns. The transit velocity depends on the deformability of the cell and the pressure at which the cells are injected. We performed three different pressure gradients (1.6/2.3/3.0 Pa/μm) by changing the heights (3.5/5/6.5 cm) between the liquid level in the injector and the inlet of the microchannel to detect the transit velocities of iRBCs. Videos of cells travelling through the microchannel were recorded, and the transit velocities of a cell passing through the microchannel were analyzed with Image J and GraphPad Prism (version 10.2.3).

1.9 STORM imaging

The purified schizont-infected erythrocytes were adhered to poly-L-lysine-coated glass coverslips, fixed by 4% paraformaldehyde and immunolabeled for tropomodulin (TMOD) by anti-TMOD antibody (OriGene, TA503146) and Alexa Fluor 647-conjugated secondary antibody (Thermo Fisher Scientific, A-31571). STORM imaging was carried out by a commercial dSTORM system (Nano-Microimaging, STORM Ultra300) based on an inverted fluorescence microscope (Nikon, Ti2-E) equipped with a 100 × oil-immersion objective (Nikon CFI Plan Apochromat λ, NA 1.49), and data were processed as previously described^[21]. TMOD was labelled to display actin-based junctional complexes as individual clusters in the STORM images, the cluster densities and distances between adjacent clusters of iRBC were calculated.

1.10 Determination of parasite growth and its ability in induction of experimental cerebral malaria

Ten WT or *Pbsbp1* Δ-infected erythrocytes were injected intravenously into the BALB/c mice ($n=5$ mice/group). Parasitemia was monitored daily for 12 days using Giemsa-stained blood smears, and parasite growth curves were plotted. For the construction of experimental cerebral malaria (ECM) models, C57BL/6 mice (female, 6 – 8 weeks) were infected intravenously with 1×10^4 WT, 1×10^4 or 5×10^4 *Pbsbp1* Δ parasites. The infected mice were monitored daily for signs of cerebral malaria, classified into five clinical stages as previously described: 1=no signs; 2=ruffled fur/abnormal posture; 3=lethargy; 4=reduced responsiveness to stimulation/ataxia/respiratory distress/hyperventilation; 5=prostration/paralysis/convulsions^[22]. Mice were classified as ECM at stage 4/5, otherwise were classified as non-cerebral malaria (NCM). The incidence and mortality rates of ECM in mice infected with WT or *Pbsbp1* Δ parasites were statistically analyzed, and survival curves were performed. To assess blood-brain barrier integrity, C57BL/6 mice diagnosed with ECM were injected intravenously with 200 μl of 2% Evans blue solution (in 1×PBS). One hour after injection, mice were euthanized and perfused transcardially with 60 ml of 1×PBS. The brain of each mouse was harvested and weighed, and subsequently incubated in 1 ml of formamide for 48 h at 37°C. The optical density (OD)

of extracted Evans blue dye was measured using a spectrophotometer at 630 nm. Evans blue extravasation of the brain was calculated as Evans blue dye (mg)/brain tissue (g) based on a standard curve.

1.11 Statistical analysis

Data are presented as mean ± standard deviation. Unpaired two-tailed *t* test was used to compare two groups. One-way ANOVA with Tukey's multiple comparisons test was used for comparisons between more than two groups. Two-way ANOVA followed by Tukey's multiple comparisons test was performed to compare multiple groups with two independent variables. Cumulative survival rates of the mice between two groups were assessed using Kaplan-Meier method and compared using log-rank test. $P < 0.05$ was considered statistically significant. * $P < 0.05$, ** $P < 0.01$, *** $P < 0.001$, **** $P < 0.0001$, ns, not significant. All data were analyzed by GraphPad Prism (version 10.2.3).

2 Results

2.1 *PbSBP1* is associated with protein 4.1R of erythrocyte membrane skeleton

Since previous studies have demonstrated that the exported parasite proteins contribute to remodeling of host erythrocyte membrane skeleton^[23] and *PfSBP1* interacts with protein 4.1R^[14], we assumed that *PbSBP1* may also participate in erythrocyte remodeling by interacting with cytoskeleton proteins. To test this possibility, we isolated membranes of *P. berghei*-infected RBCs and performed co-immunoprecipitation (co-IP). We developed polyclonal antibodies against *PbSBP1* to detect its protein levels. As shown in Figure 1a, recombinant *PbSBP1* was detected in proteins extracted from *E. coli* expressing *PbSBP1*-Flag. Immunoprecipitation of protein 4.1R by its specific antibody in membranes of iRBCs followed by Western blotting using anti-*PbSBP1* antibodies revealed the presence of this protein (Figure 1b). No signal was detected when this experiment was performed with normal mouse IgG as the IP antibody (Figure 1b). This result implies an association between *PbSBP1* and protein 4.1R in *P. berghei*-infected RBCs, which was consistent with previous research in *P. falciparum*^[14].

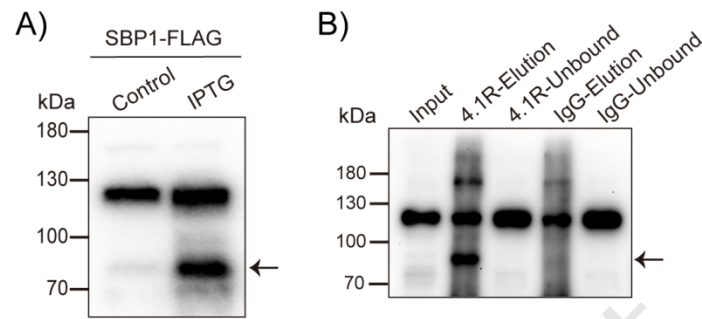


Fig.1 The association between PbsBP1 and protein 4.1R of erythrocyte membrane skeleton

(a) Detection of recombinant protein PbsBP1 expressed by *E. coli* using anti-PbsBP1 antibody. Bacterial proteins of *E. coli* transformed with the plasmid that encoded the PbsBP1-Flag protein were expressed with or without IPTG and then extracted. The arrow indicates the target band. (b) Co-immunoprecipitation of PbsBP1 with protein 4.1R. Membranes of *P. berghei*-infected RBCs were lysed and extracts were subjected to immunoprecipitation with anti-4.1R antibody or normal mouse IgG, followed by Western blotting using anti-PbsBP1 antibody. The arrow indicates the target band.

2.2 Generation of PbsBP1 Δ parasites

To explore the role of PbsBP1 in host RBC remodeling, we constructed a PbsBP1 knockout mutant by double-crossover homologous recombination (Figure 2). Plasmid pL0035-Pbsbp1 Δ was designed to disrupt PbsBP1 (PBANKA_1101300) in *P. berghei* genome (Figure 2a). Genotype of the Pbsbp1 Δ Parasites was identified by PCR and Southern blotting (Figure 2b,c). Western blotting also indicated protein loss in Pbsbp1 Δ parasites (Figure 2d).

2.3 PbsBP1 influences infected erythrocyte deformability

The shape of biconcave disks and corresponding deformability of RBC are critical features of its biological function. Erythrocyte deformability is mainly attributed to its membrane cytoskeleton network^[24]. After infection with *Plasmodium*, a number of exported proteins lead to increased rigidity of iRBCs and decreased deformability^[2, 25]. Since the membrane skeleton structure is the most critical factor to determine the deformation of erythrocytes, and PbsBP1 was found to interact with protein 4.1R and spectrin^[14], and with erythrocyte cytosolic protein LANCL1^[26], we measured deformability of Pbsbp1 Δ -infected RBCs by microfluidic approaches^[20]. Microchannels with an array of cylindrical pillars were used to detect modifications in iRBC deformability. On account of the enlarged size of the iRBC during late stages of malaria development, the distances between the rows and the columns in the

micropillar array we used were 6 μm and 10 μm (Figure 3a). At a certain pressure, the iRBCs were squashed between the rows and recovered between the columns and the transit velocity ($\mu\text{m/s}$) of iRBCs travelling through the microchannel was recorded (Figure 3b). As the pressure increased, the iRBCs passed through the microchannel more quickly (Figure 3c). Moreover, the Pbsbp1 Δ -iRBCs travelled through the microchannel significantly faster than WT-iRBCs (Figure 3b,c), indicating a reduction of rigidity in erythrocytes infected with Pbsbp1 Δ parasites. This result suggests that PbsBP1 may be involved in changes of cytoskeletal structure by interactions with skeletal proteins which contribute to increased stiffness.

2.4 PbsBP1 remodels infected erythrocytes by altering the ultrastructure of erythrocyte cytoskeleton

In order to further clarify whether PbsBP1 affects the deformability of iRBCs by altering the cytoskeleton structure of iRBCs, we performed super-resolution stochastic optical reconstruction microscopy (STORM) to compare the membrane skeleton structures of WT and Pbsbp1 Δ -iRBCs. As mentioned above, the erythrocyte cytoskeleton meshwork is composed of actin-based junctional complexes connected by spectrin tetramers, and the junction-to-junction distances or the density of junctional complexes are changed after the parasite invasion^[27]. One of the components of junctional complexes is tropomodulin (TMOD), which is

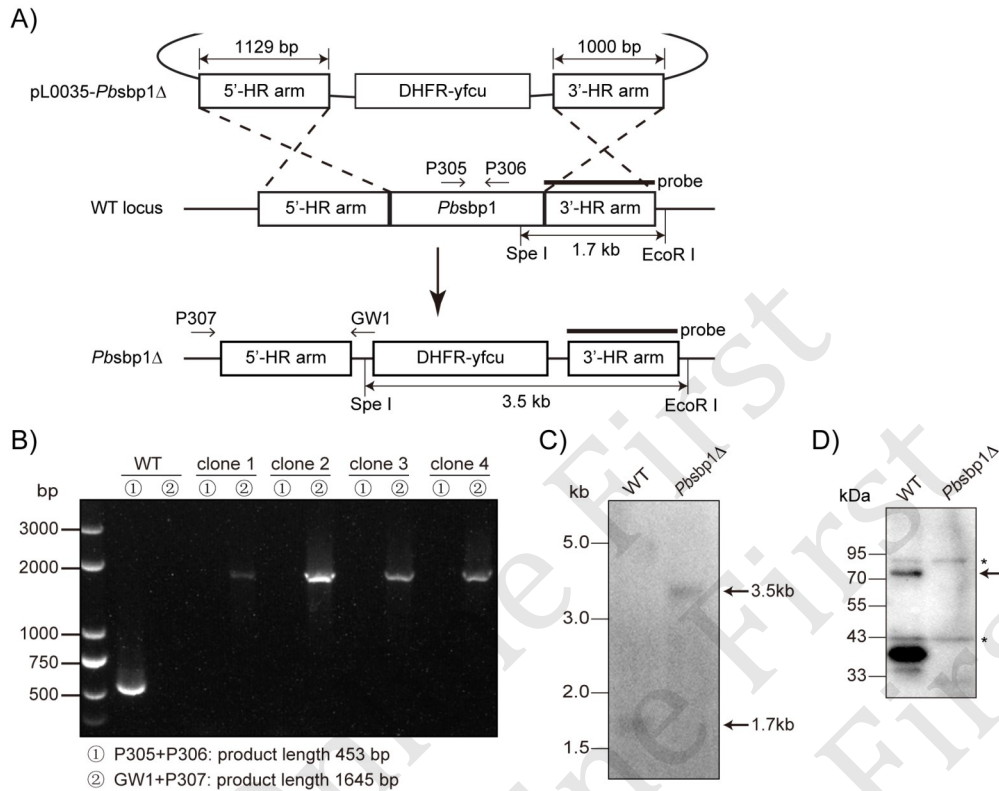


Fig.2 Deletion of *sbp1* in *P. berghei*

(a) Strategy for generation of *Pbsbp1*Δ parasites. *Pbsbp1* was replaced with an expression cassette for DHFR-yfcu using double homologous recombination. (b) PCR analysis of the *Pbsbp1*Δ mutant. The top lines indicated the WT and four independent *Pbsbp1*Δ clones. Lane 1: primers P305 and P306 (product length 453 bp). Lane 2: primers GW1 and P307 (product length 1645 bp). Specific PCR amplifications in lane 1 indicated the WT, and lane 2 indicated the expected recombination at the *sbp1* locus. (c) Southern blotting identification to confirm the modification of the *Pbsbp1* locus in *Pbsbp1*Δ parasites. SpeI and EcoRI were used to digest gDNAs of WT parasites and *Pbsbp1*Δ parasites, and probe indicated as a black bar in (a) was used for hybridization. (d) Western blotting using anti-*PbSBP1* antibody to detect *PbSBP1* in WT and *Pbsbp1*Δ parasites. The predicted molecular weight of *PbSBP1* is 90.7 ku. Asterisk represents the non-specific bands.

immunolabelled to perform STORM^[21]. TMOD labeling was displayed as individual clusters in the STORM images, the distances between adjacent clusters and the cluster densities were calculated (Figure 4). STORM imaging of schizont infected erythrocytes showed that the distances between nearest neighbors of clusters had a tendency to increase while the cluster densities were decreased in *Pbsbp1*Δ-iRBCs compared to WT-iRBCs (Figure 4c). During the asexual development of parasite inside the host erythrocyte, the actin-spectrin meshwork of the erythrocyte membrane skeleton is gradually rearranged: the length of spectrin filaments and the cytoskeleton-bilayer adherence increases, the distribution and amount of F-actin changes, the meshes expand, and large holes appear in the cytoskeleton, etc. ^[21, 28]. All these factors lead to

changes in the ability of erythrocytes to deform. Therefore, these results suggested that *PbSBP1* may influence the deformability of iRBCs by participating in the aforementioned processes that lead to changes in membrane skeleton structure.

2.5 Deletion of *PbSBP1* inhibits blood stage parasites growth and experimental cerebral malaria pathogenesis

PbSBP1 is located in the Maurer's clefts-like structures in *P. berghei* iRBCs^[15]. Maurer's clefts are essential for the trafficking and sorting of parasite proteins within the *P. falciparum* infected-RBCs, and these structures are closely related to the pathogenicity of the parasite. Therefore, we assumed that the structural remodeling of iRBCs that is mediated by *PbSBP1* is also related to its function in parasite virulence. We examined the phenotype of

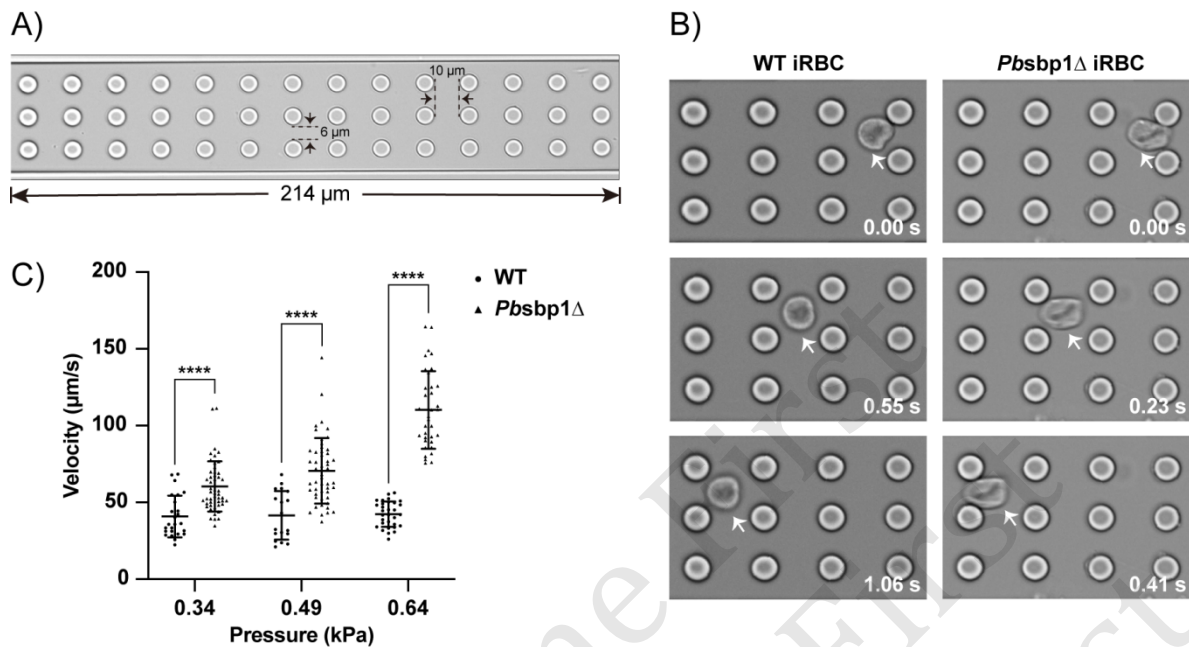


Fig.3 Increased deformability in *Pbsbp1*Δ parasite-infected erythrocytes

(a) The design of microchannel assembly. (b) Representative image sequences of WT or *Pbsbp1*Δ-infected erythrocytes travelling through the microchannel at a pressure of 0.64 kPa. The white arrow indicates the infected erythrocyte. (c) The transit velocities of WT or *Pbsbp1*Δ-infected erythrocytes travelling through the microchannel at different pressure gradients (WT: $n=18-31$; *Pbsbp1*Δ: $n=35-50$). Data are shown as mean±SD and analyzed by unpaired *t* test between the WT group and the *Pbsbp1*Δ group at the same pressure gradient. **** $P<0.0001$.

*Pbsbp1*Δ parasite in mice. BALB/c mice infected with 10 WT or *Pbsbp1*Δ-iRBCs were monitored the parasitemia for 12 d after infection. Compared to the WT group, *Pbsbp1*Δ-infected mice exhibited reduced parasitemia (Figure 5a), indicating the attenuated growth of *Pbsbp1*Δ parasites in the erythrocytic cycle. Cerebral malaria is a severe neurological complication that is responsible for the majority of malaria-related deaths^[29]. It is characterized by iRBCs sequestration in the brain, which triggers immune cell infiltration and inflammation, resulting in the damage of blood-brain barrier (BBB)^[30]. In order to further evaluate the function of *PbsBP1* in parasite virulence, we assessed the ability of *Pbsbp1*Δ parasites in induction of cerebral malaria using experimental cerebral malaria (ECM) models. C57BL/6 mice were intravenously inoculated with WT or *Pbsbp1*Δ-iRBCs (1×10^4 iRBCs/mouse). As expected, all WT-infected mice displayed signs of ECM and died within 7–10 d post infection (p. i.). In contrast, 70% of *Pbsbp1*Δ-infected mice were alive and showed no obvious signs of ECM until day 10 p. i. (Figure 5b). The growth of *Pbsbp1*Δ parasites in C57BL/6 mice was also significantly lower than that of WT parasites (Figure 5c). Since

increased permeability of the BBB is a typical feature of cerebral malaria, the integrity of the BBB of WT or *Pbsbp1*Δ-infected mice was examined using Evans blue staining of brain tissue. The brain tissues of the infected mice were collected when the mice were diagnosed as ECM, otherwise, the mice with no obvious ECM signs were classified as non-cerebral malaria (NCM) and the brains of which were collected at day 10 p.i.. The integrity of BBB in brains of *Pbsbp1*Δ-infected mice was not severely damaged compared with WT-infected mice (Figure 5d), which was consistent with the incidence rate of ECM. In order to exclude parasite load-linked differences in ECM, we tested a higher infectious dose of *Pbsbp1*Δ (5×10^4 iRBCs/mouse). All the mice infected with 5×10^4 *Pbsbp1*Δ-iRBCs were alive and showed no obvious signs of ECM until day 10 p.i. (Figure 5e), and the parasitemia of these mice was notably higher than that of the 1×10^4 *Pbsbp1*Δ-iRBCs infected mice, and increased to a similar parasitemia of the WT group at day 10 p.i. (Figure 5f). The integrity of BBB in brains of *Pbsbp1*Δ-infected mice (5×10^4 iRBCs/mouse) was not severely damaged compared with WT-infected mice (Figure 5g), which was consistent with

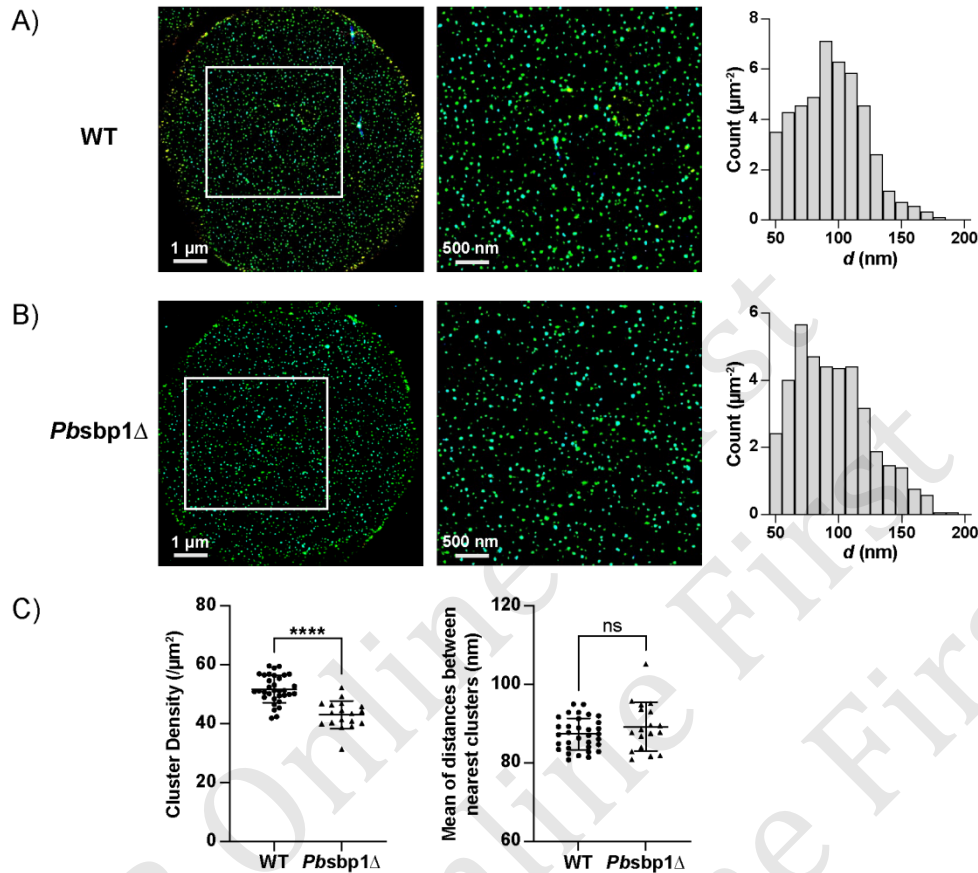


Fig.4 STORM results of actin-capping protein tropomodulin in WT or *Pbsbp1*Δ-infected erythrocytes

(a) STORM image of tropomodulin at low and high magnifications and distribution of distances between nearest neighbors of clusters in WT iRBC. (b) STORM image of tropomodulin at low and high magnifications and distribution of distances between nearest neighbors of clusters in *Pbsbp1*Δ iRBC. (c) The mean junction-to-junction distances of *Pbsbp1*Δ-infected erythrocytes had a tendency to increase while the cluster densities significantly decreased compared to WT-infected erythrocytes (WT: $n=33$; *Pbsbp1*Δ: $n=19$). Data are shown as mean±SD and analyzed by unpaired *t* test between the WT group and the *Pbsbp1*Δ group. **** $P<0.0001$, ns, not significant.

the incidence rate of ECM. These results demonstrate that *PbSBP1* may affect the virulence of the malaria parasite by regulating the cytoskeleton structure of infected erythrocytes, and the attenuated ability of *Pbsbp1*Δ parasites in inducing ECM is mainly due to the reduced pathogenicity rather than the consequence of lower parasite load.

3 Discussion

SBP1 is a *Plasmodium* export element (PEXEL)-negative exported protein, and is conserved between *P. falciparum* and rodent malarial^[15]. *PfSBP1* contains one transmembrane domain, which is trafficked and inserted into the membrane of Maurer's cleft with its N-terminus facing the lumen side of the cleft and C-terminus facing the RBC cytoplasm^[31]. The domain

structure of *PbSBP1* is similar to *PfSBP1*, and *PbSBP1* is located in Maurer's clefts-like structures in *P. berghei* iRBC^[16]. Maurer's clefts are mobile in the ring stage iRBC cytoplasm while later become tethered to the iRBC membrane skeleton through the interaction of parasite proteins and cytoskeleton proteins^[32]. Since most studies of SBP1 were focused on *P. falciparum*, we first found that *PbSBP1* was associated with RBC skeleton protein 4.1R by co-IP. To investigate the role of *PbSBP1* in RBC remodeling, we generated the *Pbsbp1* gene-deletion mutant in *P. berghei* and anti-*PbSBP1* polyclonal antibody. As we expected, the deformability of *Pbsbp1*Δ-iRBCs was improved compared to WT-iRBCs, indicating *PbSBP1* may participate in modification of erythrocyte membrane skeleton network. Maurer's

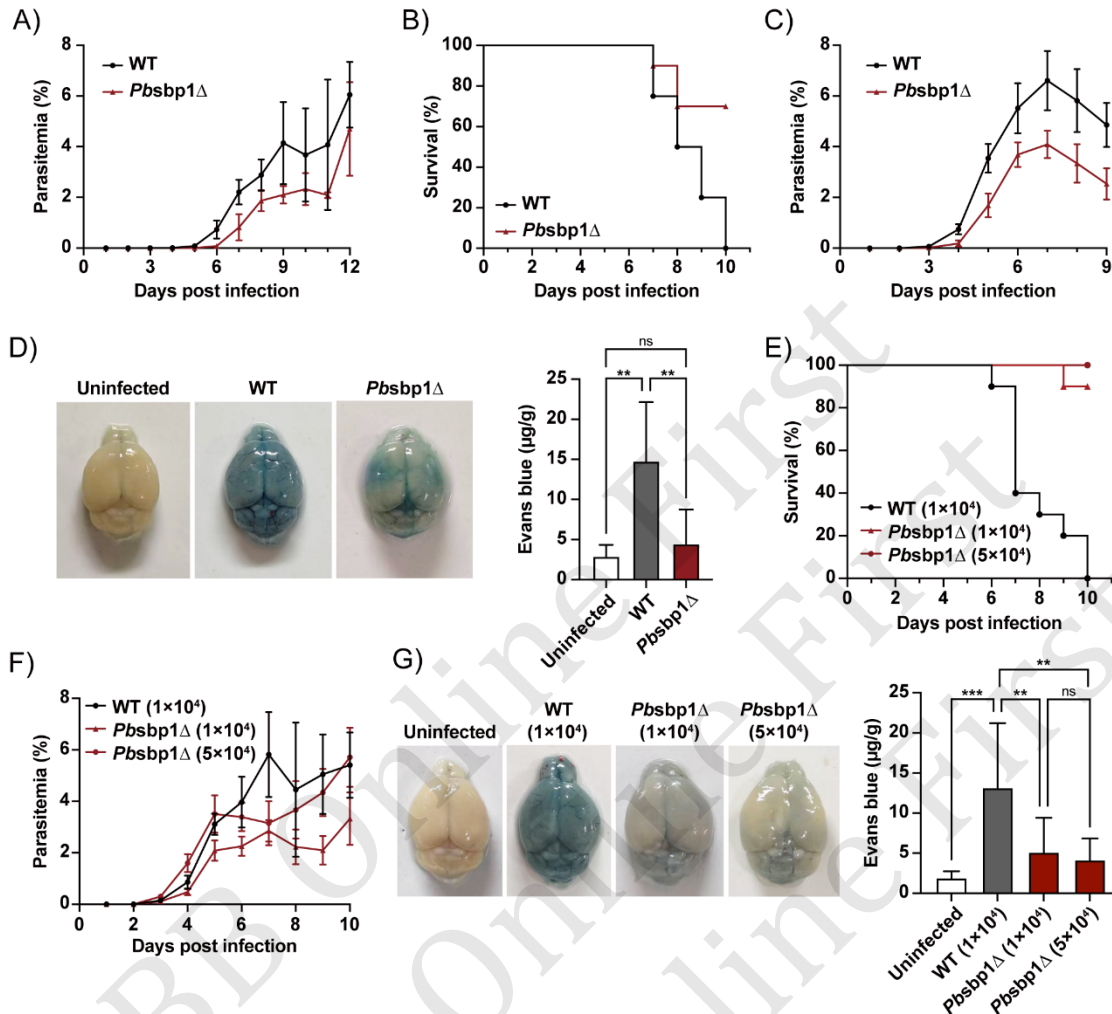


Fig.5 Loss of *PbsBP1* leads to reduced blood stage growth and ECM incidence

(a) Growth curves of WT and *Pbsbp1*Δ parasites in BALB/c mice ($n=5$ mice/group) reveal that *PbsBP1*'s deletion reduces parasite growth in the asexual cycle. $P<0.05$. (b) Survival of C57BL/6 mice infected with 1×10^4 WT or *Pbsbp1*Δ parasites ($n=8-10$ mice/group). Survival rate was significantly higher in *Pbsbp1*Δ-infected mice than in WT-infected mice. $P<0.01$. (c) The course of parasitemia of C57BL/6 mice ($n=8-10$ mice/group) in (b). Significant differences in parasitemia were detected between WT and *Pbsbp1*Δ-infected mice. $P<0.0001$. (d) Left panel: Representative images of brains from mice infected with WT or *Pbsbp1*Δ parasites and injected with Evans blue to detect BBB leakage. Right panel: Quantification of Evans blue in brains showed significant differences in the integrity of BBB between WT and *Pbsbp1*Δ-infected mice ($n=7-8$ mice/group). The uninfected mice were used as controls ($n=6$ mice/group). (e) Survival of C57BL/6 mice infected with WT (1×10^4) or *Pbsbp1*Δ (1×10^4 or 5×10^4) parasites ($n=10$ mice/group). Survival rate was significantly higher in *Pbsbp1*Δ-infected mice than in WT-infected mice. $P<0.0001$. (f) The course of parasitemia of C57BL/6 mice in (e). Significant differences in parasitemia were detected between WT and high dose *Pbsbp1*Δ-infected mice ($P<0.05$), and between the two groups of mice infected with *Pbsbp1*Δ parasites ($P<0.0001$). (g) Left panel: Representative images of brains from mice infected with WT or *Pbsbp1*Δ parasites and injected with Evans blue to detect BBB leakage. Right panel: Quantification of Evans blue in brains showed significant differences in the integrity of BBB between WT and two groups of *Pbsbp1*Δ-infected mice ($n=9-10$ mice/group). The uninfected mice were used as controls ($n=6$ mice/group). Data are shown as mean \pm SD (a, c, d, f, g) and were analyzed by two-way ANOVA with Tukey's multiple comparisons test (a, e, f) and one-way ANOVA with Tukey's multiple comparisons test (d, g). Log-rank test from Kaplan-Meier survival curve was performed between the WT group and the *Pbsbp1*Δ group (b, e). ** $P<0.01$, *** $P<0.001$, ns, not significant.

clefts are important for the sorting of parasite proteins in the iRBCs^[33], and *PfSBP1* is essential for the translocation of *PfEMP1* from Maurer's cleft onto the

surface of iRBCs^[34]. Although there is no homologous protein of *PfEMP1* in *Plasmodium berghei*, and its infection of RBCs does not form knob structures,

given that *PbSBP1* is also located in Maurer's clefts-like structures in *Plasmodium berghei*, it is very likely to have a similar function. Hence, the improvement of *Pbsbp1* Δ -iRBCs' rigidity may also be due to the change of trafficking virulence factors to the iRBCs surface. Furthermore, we examined the structural organization of cytoskeleton in WT and *Pbsbp1* Δ iRBCs, and found *sbp1* knockout indeed caused changes in the distribution of actin-based junctional complexes. The C-terminus of *PfSBP1* has been proved to bind with protein 4.1R and α -spectrin in *in vitro* assay^[14], and an erythrocyte cytosolic protein LANCL1 is recruited to the surface of Maurer's clefts and interacts with *PfSBP1*^[26]. Taking into account the conservation of SBP1 across different species of *Plasmodium*, our results demonstrate that SBP1 in *P. berghei* may also interact directly or indirectly with cytoskeletal proteins or other proteins of iRBCs to remodel erythrocytes, which need further *in vitro* experiments to verify. It is reported that *PbSBP1* is required for iRBC sequestration in the adipose tissue and lungs, and *Pbsbp1* Δ parasites displayed an attenuated phenotype in mice^[15]. In this study, we also observed the reduced growth rates of *Pbsbp1* Δ parasites compared with WT parasites in both BALB/c and C57BL/6 mice. Utilizing the ECM model, we found that the permeability of blood-brain barrier of *Pbsbp1* Δ -infected mice was significantly improved even when infected with a higher dose of parasites. Therefore, the attenuated phenotype of *Pbsbp1* Δ parasites may be associated with the changes of iRBC cytoskeleton, and with impairment of the export of malaria parasite proteins.

4 Conclusion

Our findings underscore the role of SBP1 in remodeling of parasite-infected erythrocytes. We demonstrate an association between *PbSBP1* and host erythrocyte cytoskeleton protein 4.1R, and further establish the importance of *PbSBP1* in deformability and ultrastructure of cytoskeleton network in iRBCs. Furthermore, the cytoskeleton remodeling of iRBC mediated by *PbSBP1* is associated with the pathogenicity of the parasite. The conservation of protein trafficking machinery and SBP1 across *P. falciparum* and rodent malaria species supports the utility of *P. berghei* as a model system for investigating host cell remodeling and parasite

virulence.

References

- [1] Lux S E 4th. Anatomy of the red cell membrane skeleton: unanswered questions. *Blood*, 2016, **127**(2): 187-199
- [2] Warncke J D, Beck H P. Host cytoskeleton remodeling throughout the blood stages of *Plasmodium falciparum*. *Microbiol Mol Biol Rev*, 2019, **83**(4): e00013-e00019
- [3] Pei X, Guo X, Coppel R, *et al.* The ring-infected erythrocyte surface antigen (RESA) of *Plasmodium falciparum* stabilizes spectrin tetramers and suppresses further invasion. *Blood*, 2007, **110**(3): 1036-1042
- [4] Waller K L, Nunomura W, An X, *et al.* Mature parasite-infected erythrocyte surface antigen (MESA) of *Plasmodium falciparum* binds to the 30-kDa domain of protein 4.1 in malaria-infected red blood cells. *Blood*, 2003, **102**(5): 1911-1914
- [5] Black C G, Proellocks N I, Kats L M, *et al.* *In vivo* studies support the role of trafficking and cytoskeletal-binding motifs in the interaction of MESA with the membrane skeleton of *Plasmodium falciparum*-infected red blood cells. *Mol Biochem Parasitol*, 2008, **160**(2): 143-147
- [6] Weng H, Guo X, Papoin J, *et al.* Interaction of *Plasmodium falciparum* knob-associated histidine-rich protein (KAHRP) with erythrocyte ankyrin R is required for its attachment to the erythrocyte membrane. *Biochim Biophys Acta*, 2014, **1838**(1 Pt B): 185-192
- [7] Pei X, An X, Guo X, *et al.* Structural and functional studies of interaction between *Plasmodium falciparum* knob-associated histidine-rich protein (KAHRP) and erythrocyte spectrin. *J Biol Chem*, 2005, **280**(35): 31166-31171
- [8] Oh S S, Voigt S, Fisher D, *et al.* *Plasmodium falciparum* erythrocyte membrane protein 1 is anchored to the actin-spectrin junction and knob-associated histidine-rich protein in the erythrocyte skeleton. *Mol Biochem Parasitol*, 2000, **108**(2): 237-247
- [9] Waller K L, Stubberfield L M, Dubljevic V, *et al.* Interactions of *Plasmodium falciparum* erythrocyte membrane protein 3 with the red blood cell membrane skeleton. *Biochim Biophys Acta*, 2007, **1768**(9): 2145-2156
- [10] Oberli A, Zurbrugg L, Rusch S, *et al.* *Plasmodium falciparum* Plasmodium helical interspersed subtelomeric proteins contribute to cytoadherence and anchor *P. falciparum* erythrocyte membrane protein 1 to the host cell cytoskeleton. *Cell Microbiol*, 2016, **18**(10): 1415-1428
- [11] Waller K L, Stubberfield L M, Dubljevic V, *et al.* Interaction of the exported malaria protein Pf332 with the red blood cell membrane skeleton. *Biochim Biophys Acta*, 2010, **1798**(5): 861-871
- [12] Shakya B, Penn W D, Nakayasu E S, *et al.* The *Plasmodium falciparum* exported protein PF₃D7_0402000 binds to erythrocyte ankyrin and band 4.1. *Mol Biochem Parasitol*, 2017, **216**: 5-13
- [13] Shakya B, Kilili G K, Wang L, *et al.* Identification of exported *Plasmodium falciparum* proteins that bind to the erythrocyte

- cytoskeleton. *Microorganisms*, 2022, **10**(7): 1438
- [14] Kats L M, Proellocks N I, Buckingham D W, *et al.* Interactions between *Plasmodium falciparum* skeleton-binding protein 1 and the membrane skeleton of malaria-infected red blood cells. *Biochim Biophys Acta*, 2015, **1848**(7): 1619-1628
- [15] De Niz M, Ullrich A K, Heiber A, *et al.* The machinery underlying malaria parasite virulence is conserved between rodent and human malaria parasites. *Nat Commun*, 2016, **7**: 11659
- [16] Ingmundson A, Nahar C, Brinkmann V, *et al.* The exported *Plasmodium berghei* protein IBIS1 delineates membranous structures in infected red blood cells. *Mol Microbiol*, 2012, **83**(6): 1229-1243
- [17] Fonager J, Pasini E M, Braks J A, *et al.* Reduced CD36-dependent tissue sequestration of *Plasmodium*-infected erythrocytes is detrimental to malaria parasite growth *in vivo*. *J Exp Med*, 2012, **209**(1): 93-107
- [18] Janse C J, Ramesar J, Waters A P. High-efficiency transfection and drug selection of genetically transformed blood stages of the rodent malaria parasite *Plasmodium berghei*. *Nat Protoc*, 2006, **1**(1): 346-356
- [19] Shi X, Hai L, Govindasamy K, *et al.* A *Plasmodium* homolog of ER tubule-forming proteins is required for parasite virulence. *Mol Microbiol*, 2020, **114**(3): 454-467
- [20] Xing F, Xun S, Zhu Y, *et al.* Microfluidic assemblies designed for assessment of drug effects on deformability of human erythrocytes. *Biochem Biophys Res Commun*, 2019, **512**(2): 303-309
- [21] Pan L, Yan R, Li W, *et al.* Super-resolution microscopy reveals the native ultrastructure of the erythrocyte cytoskeleton. *Cell Rep*, 2018, **22**(5): 1151-1158
- [22] Villegas-Mendez A, Greig R, Shaw T N, *et al.* IFN- γ -producing CD4⁺ T cells promote experimental cerebral malaria by modulating CD8⁺ T cell accumulation within the brain. *J Immunol*, 2012, **189**(2): 968-979
- [23] Maier A G, Cooke B M, Cowman A F, *et al.* Malaria parasite proteins that remodel the host erythrocyte. *Nat Rev Microbiol*, 2009, **7**(5): 341-354
- [24] Tutwiler V. To deform or not to deform: the evolutionary basis of mammalian red blood cell deformability. *Biophys J*, 2021, **120**(17): 3539-3540
- [25] Maier A G, Rug M, O'Neill M T, *et al.* Exported proteins required for virulence and rigidity of *Plasmodium falciparum*-infected human erythrocytes. *Cell*, 2008, **134**(1): 48-61
- [26] Blisnick T, Vincensini L, Barale J C, *et al.* LANCL1, an erythrocyte protein recruited to the Maurer's clefts during *Plasmodium falciparum* development. *Mol Biochem Parasitol*, 2005, **141**(1): 39-47
- [27] Shi H, Liu Z, Li A, *et al.* Life cycle-dependent cytoskeletal modifications in *Plasmodium falciparum* infected erythrocytes. *PLoS One*, 2013, **8**(4): e61170
- [28] Kwon S, Lee D H, Han S J, *et al.* Biomechanical properties of red blood cells infected by *Plasmodium berghei* ANKA. *J Cell Physiol*, 2019, **234**(11): 20546-20553
- [29] Luzolo A L, Ngoyi D M. Cerebral malaria. *Brain Res Bull*, 2019, **145**: 53-58
- [30] Gillrie M R, Lee K, Gowda D C, *et al.* *Plasmodium falciparum* histones induce endothelial proinflammatory response and barrier dysfunction. *Am J Pathol*, 2012, **180**(3): 1028-1039
- [31] Iriko H, Ishino T, Tachibana M, *et al.* Skeleton binding protein 1 (SBP1) of *Plasmodium falciparum* accumulates in electron-dense material before passing through the parasitophorous vacuole membrane. *Parasitol Int*, 2020, **75**: 102003
- [32] McMillan P J, Millet C, Batinovic S, *et al.* Spatial and temporal mapping of the PfEMP1 export pathway in *Plasmodium falciparum*. *Cell Microbiol*, 2013, **15**(8): 1401-1418
- [33] Mundwiler-Pachlatko E, Beck H P. Maurer's clefts, the enigma of *Plasmodium falciparum*. *Proc Natl Acad Sci U S A*, 2013, **110**(50): 19987-19994
- [34] Cooke B M, Buckingham D W, Glenister F K, *et al.* A Maurer's cleft-associated protein is essential for expression of the major malaria virulence antigen on the surface of infected red blood cells. *J Cell Biol*, 2006, **172**(6): 899-908

*PbSBP1*影响伯氏疟原虫感染红细胞膜骨架结构和变形能力*

郭欣悦¹⁾ 赵焕琪¹⁾ 钟燕璇¹⁾ 姜如梦¹⁾ 李耀先²⁾ 潘雷霆²⁾ 王倩^{1)**} 史小雨^{1)**}

¹⁾ 天津医科大学基础医学院免疫学系, 天津市细胞与分子免疫学重点实验室, 免疫微环境与疾病教育部重点实验室, 天津 300070;

²⁾ 南开大学物理学院, 泰达应用物理研究院, 弱光非线性光子学教育部重点实验室, 天津 300071)

摘要 目的 疟原虫通过输出蛋白质与宿主红细胞膜骨架蛋白相互作用, 从而重塑红细胞结构, 以维持其胞内寄生及致病性。骨架结合蛋白1 (SBP1) 是一种疟原虫输出蛋白, 在不同疟原虫种属中高度保守。研究表明, 恶性疟原虫 SBP1 与感染红细胞膜骨架蛋白相互作用, 但该蛋白质在伯氏疟原虫 (*Plasmodium berghei*, *Pb*) 中的作用尚未阐明。本研究计划探究 *PbSBP1* 在宿主红细胞重塑及疟原虫致病性中的作用。**方法** 在伯氏疟原虫中, 通过免疫共沉淀方法探究 *PbSBP1* 与红细胞膜骨架蛋白4.1R的关系。基于双臂同源重组原理构建 *Pbsbp1* 基因敲除的伯氏疟原虫突变体 (*Pbsbp1*Δ), 通过微流控方法分析 *Pbsbp1*Δ 疟原虫感染红细胞的变形能力, 对红细胞膜骨架连接复合体成分原肌球蛋白调节蛋白进行荧光标记, 对疟原虫感染红细胞骨架网络进行超分辨率随机光学重建显微镜成像, 分析 *Pbsbp1*Δ 感染红细胞骨架超微结构的变化。进一步利用患疟鼠模型和小鼠脑型疟疾模型, 监测红内期 *Pbsbp1*Δ 疟原虫生长情况及其诱导小鼠发生脑型疟疾的能力。**结果** *PbSBP1* 可能通过与红细胞膜骨架蛋白4.1R的直接或间接的相互作用, 参与感染红细胞的重塑。微流控结果显示, *Pbsbp1*Δ 疟原虫感染红细胞的变形能力较野生型疟原虫感染红细胞显著增强。超分辨率随机光学重建显微镜成像结果表明, *Pbsbp1*Δ 感染红细胞骨架超微结构较野生型感染红细胞发生变化。进一步表型分析发现, 红内期 *Pbsbp1*Δ 疟原虫生长速度较野生型疟原虫显著减慢, 其诱导小鼠发生脑型疟疾的能力也降低。上述结果提示, *PbSBP1* 可能通过与4.1R蛋白的相互作用, 参与感染红细胞膜骨架的重塑, 从而调节感染红细胞的变形性, 并影响红内期疟原虫的致病性。**结论** 本研究阐明了 *PbSBP1* 在宿主红细胞重塑及疟原虫致病性中的作用, 为疟疾的防治提供理论基础和新的研究思路。

关键词 *PbSBP1*, 红细胞重塑, 细胞骨架超微结构, 红细胞变形能力

中图分类号 R382.3+1

DOI: 10.3724/j.pibb.2026.0010

CSTR: 32369.14.pibb.20260010

* 国家自然科学基金 (32200976, 32070701) 资助项目。

** 通讯联系人。

王倩 Tel: 022-83336817, E-mail: wangq@tmu.edu.cn

史小雨 Tel: 022-83336817, E-mail: shixy@tmu.edu.cn

收稿日期: 2026-01-06, 接受日期: 2026-03-01